Preprint
UCRL-JC-148110

100-Picometer Interferometry for EUVL

G.E. Sommargren, S.W. Phillion, M.A. Johnson, N.Q. Nguyen, A. Barty, F.J. Snell, D.R. Dillon, L.A. Bradsher

This article was submitted to The International Society for Optical Engineering, Microlithography 2002, Santa Clara, CA, March 3-6, 2002

March 18, 2002

U.S. Department of Energy

Lawrence
Livermore
National
Laboratory

This work was performed under the auspices of the United States Department of Energy by the University of California, Lawrence Livermore National Laboratory under contract No. W-7405-Eng-48.

100-picometer interferometry for EUVL

Gary E. Sommargren, Donald W. Phillion, Michael A. Johnson, Nhan Q. Nguyen, Anton Barty, Franklyn J. Snell, Daren R. Dillon, Lloyd S. Bradsher
Lawrence Livermore National Laboratory, University of California

ABSTRACT

Future extreme ultraviolet lithography (EUVL) steppers will, in all likelihood, have six-mirror projection cameras. To operate at the diffraction limit over an acceptable depth of focus each aspheric mirror will have to be fabricated with an absolute figure accuracy approaching 100pm rms. We are currently developing visible light interferometry to meet this need based on modifications of our present phase shifting diffraction interferometry (PSDI) methodology where we achieved an absolute accuracy of 250pm. The basic PSDI approach has been further simplified, using lensless imaging based on computational diffractive back-propagation, to eliminate auxiliary optics that typically limit measurement accuracy. Small remaining error sources, related to geometric positioning, CCD camera pixel spacing and laser wavelength, have been modeled and measured. Using these results we have estimated the total system error for measuring off-axis aspheric EUVL mirrors with this new approach to interferometry.

Keywords: Extreme ultraviolet lithography, aspheric mirrors, interferometry

1. INTRODUCTION

The projection optics for EUVL are based on all reflective ring-field imaging systems made up of three or more off-axis multilayer-coated aspheric mirrors. If these projection systems are to achieve diffraction limited performance, the deviation of the wavefront from spherical in the exit pupil must be less than $\lambda/14$ rms where $\lambda = 13.4$nm is the operating wavelength. The wavefront error must therefore be less than 1.0nm rms. If the imaging system is made up of four mirrors, the error contribution from each mirror can be no larger than 0.50nm rms (assuming uncorrelated errors), or 0.25nm rms surface figure error (due to the doubling of the error on reflection). For more advanced designs using additional mirrors, the permissible surface error is even smaller. For a six-mirror projection system the surface figure error drops to 0.20nm rms. To ensure the full use of the depth of focus, the requirements on the mirrors will actually be closer to 0.15nm rms. This will require metrology with 0.10nm, or 100pm, accuracy.

Fabrication of these mirrors requires real-time metrology to serve as the feedback mechanism for the finishing process. This metrology must: 1) be suitable for bare glass surfaces; 2) have a range of tens of μm; and 3) have an accuracy of 100pm. Interferometry using visible light satisfies the first two requirements. The last requirement is more difficult to attain with standard interferometry. To achieve the required measurement accuracy on aspheric mirrors, the phase shifting diffraction interferometer was developed. It is based on using diffraction to generate near-perfect spherical measurement and reference wavefronts and on minimizing the number of critical components that limit accuracy, including elimination of a reference surface and most of the auxiliary optics.

2. PHASE SHIFTING DIFFRACTION INTERFEROMETRY

The phase shifting diffraction interferometer[1] (PSDI) described here is based on diffraction. Diffraction is a fundamental process that permits the generation of near-perfect spherical wavefronts over a specific numerical aperture by using a circular aperture with a radius comparable to the wavelength of light λ_v. The sphericity of the wavefronts depends on the diameter, circularity, thickness and material properties of the diffracting aperture. Symmetry and homogeneity are key to producing diffracting apertures suitable for 100pm interferometry. Using this principle, two independent wavefronts can be generated—one serves as the measurement wavefront and is incident on the optic or optical system under test and the other serves as the reference wavefront. Since they are generated independently their relative amplitudes and phases can be controlled, providing contrast adjustment and phase shifting capability. This concept can be implemented in several

different ways. The one described here is based on single-mode optical fibers and lithographically prepared diffraction apertures that provide the diffracted wavefronts.

Fig. 1 shows the PSDI configured for measuring the surface figure of a concave off-axis aspheric mirror. The light source is a short-coherence-length (~2mm) laser operating at λ_v = 532nm. The output beam is divided by a polarization beamsplitter. One beam is reflected from a retroreflector mounted on a piezoelectric phase shifter[2] and the other beam is reflected from a retroreflector mounted on a variable delay line. The two beams are recombined by the beamsplitter and launched into a single-mode optical fiber. The end of the fiber is placed on the optical axis of the mirror at an axial position that minimizes the slope of the aspheric departure over the clear aperture of the mirror. The delay path-length is set equal to the round-trip distance from the fiber to the mirror. The spherical wavefronts diffracted from the end of the

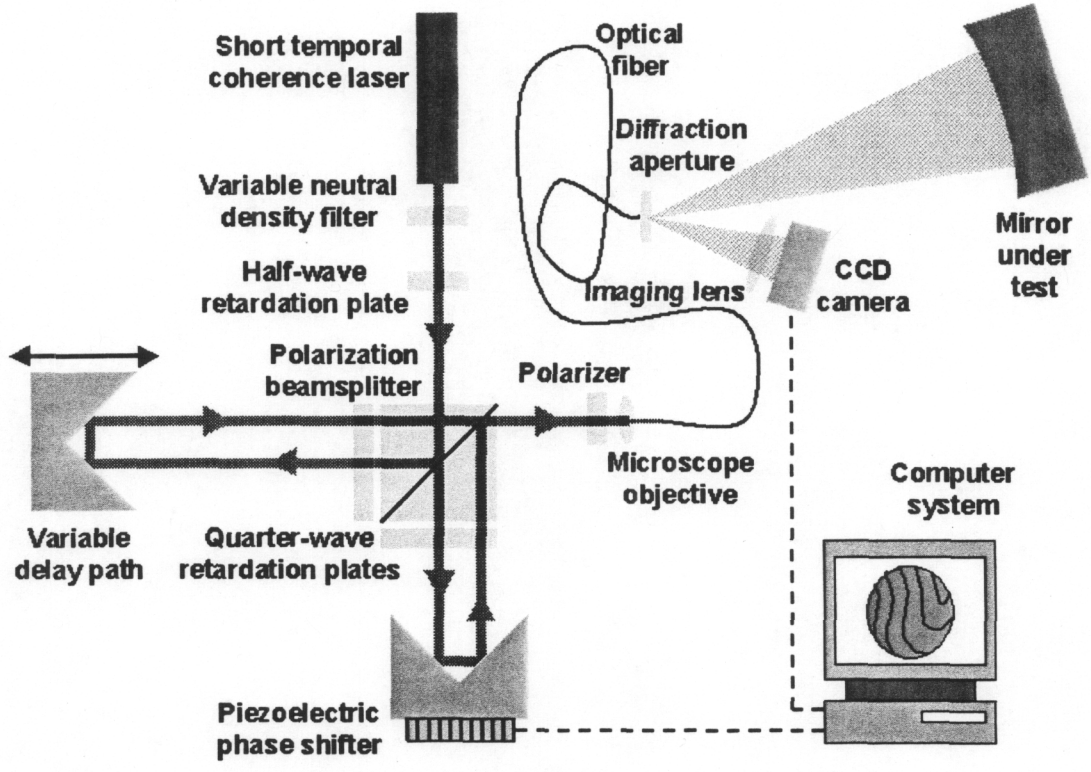

Fig. 1. PSDI configured to measure the surface figure of a concave off-axis aspheric mirror.

fiber have sufficient numerical aperture to illuminate both the mirror and imaging lens. The phase-shifted wavefront reflected from the mirror is focused back onto the diffraction aperture substrate as shown in Fig. 2 and then reflected from the coating on the substrate, combining with the delayed diffracted wavefront. Since the optical path difference between these wavefronts is precisely zero, the wavefronts are temporally coherent and interfere. Extraneous wavefronts from the interferometer are temporally incoherent and do not interfere with the primary wavefronts. Extraneous wavefronts do however add a background and thereby reduce the visibility of the fringes produced by the interfering wavefronts. Interference is observed in the image plane of the aspheric mirror with a CCD camera.

Fig. 3a shows the interference pattern of an off-axis aspheric EUVL mirror (designated M4) on which the null fringe is positioned to minimize fringe density (not necessarily the best-fit sphere). The aspheric departure from a sphere of this particular mirror is approximately 5.9μm. The phase is determined using phase shifting measurement techniques and phase extraction algorithms[3]. The surface figure error in the mirror, shown in Fig. 3b, is found by subtracting the theoretical aspheric equation that defines the perfect mirror from the measured phase.

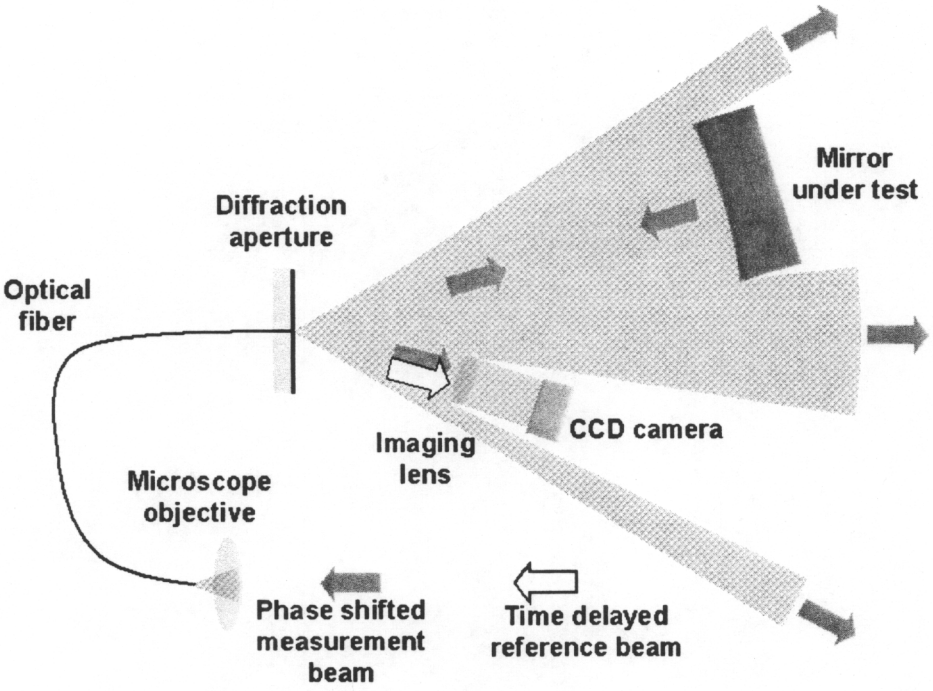

Fig. 2. Detail of the diffracted and reflected wavefronts at the end of the fiber.

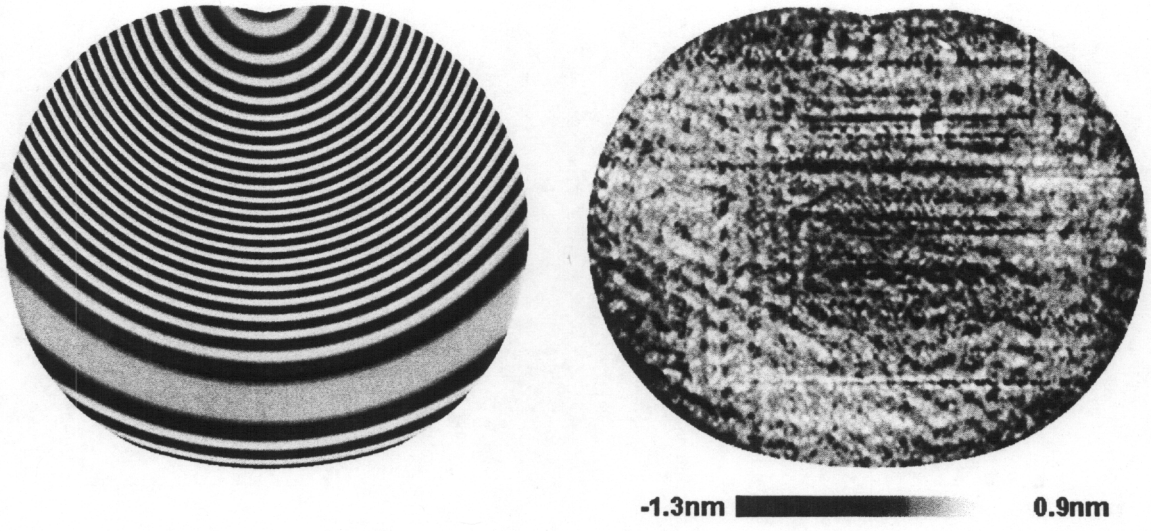

(a) (b)

Fig. 3. (a) Interferogram of a concave off-axis aspheric EUVL mirror M4. (b) The departure from the theoretical asphere is 0.24nm rms.

This particular configuration has been used for figure metrology during the fabrication of many aspheric mirrors for EUVL projection cameras. The measurement accuracy of this configuration is ~0.25nm rms, as determined by the intercomparison of measurements made with different PSDIs of the same mirror. This accuracy was sufficient for the current generation of EUVL optics but will not meet the requirements for future lithography tools having six-mirror projection cameras, which will have a single-pass wavefront of $\lambda/25$ (λ~13.4nm) to maximize process latitude. Each mirror will then have to be fabricated with a surface figure error no larger than 0.11nm rms, assuming the surface errors on the mirrors are uncorrelated and the factor of two, due to reflection, has been taken into account.

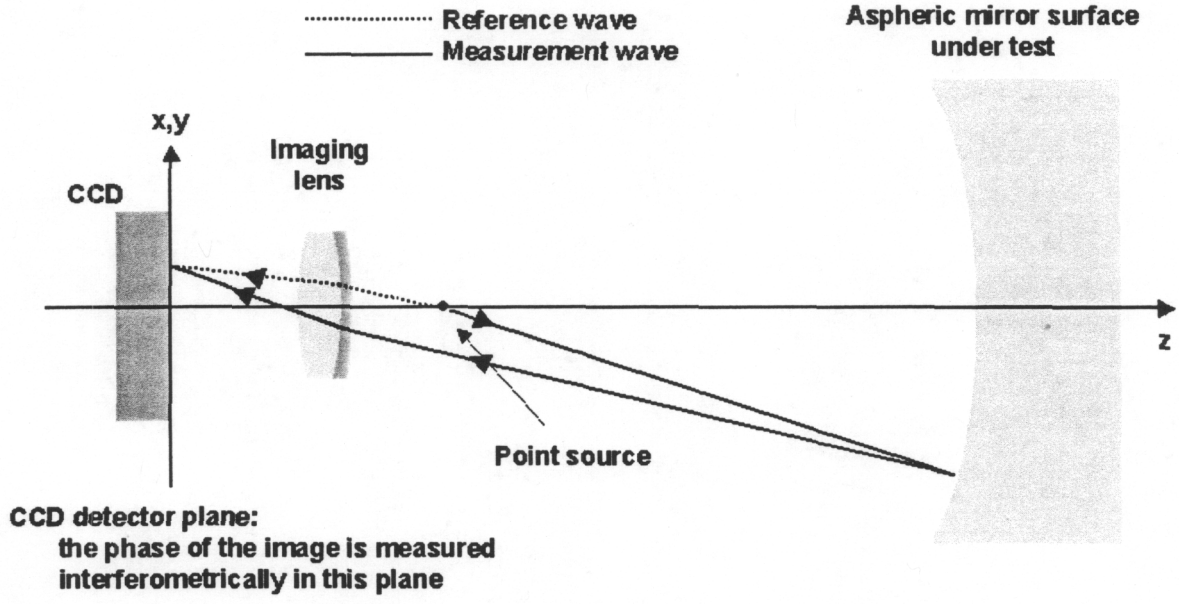

Fig. 4. Unfolded layout of a PSDI with an imaging lens.

The accuracy of the present PSDIs is limited by a number of error sources, the largest being associated with the imaging lens. Although the imaging system for a PSDI is specifically designed for the particular aspheric mirror to be tested, there are a number of error sources that are difficult to control or characterize. An unfolded layout of a PSDI is shown in Fig. 4. The paths of the measurement and reference wavefronts are shown for an arbitrary ray pair that interfere at the CCD. For an aspheric mirror these rays are non-common path as they pass through the imaging lens. Optical path differences due to the imaging lens design, fabrication errors, surface roughness, coatings, dust particles, alignment, and birefringence are subtle but significant at the 100pm rms level. There is also the problem of image distortion, which causes an error in the coordinate mapping from the mirror under test to the CCD and ultimately leads to surface figure error. Correcting for distortion is difficult because it depends on placing the CCD at the correct image plane, which is not easy to do experimentally. Some of these errors are described in more detail in Ref. 4.

3. LENSLESS PSDI

Removal of the imaging lens would eliminate the most significant error sources in the PSDI. This can de achieved by replacing the function of the lens with numerical calculations based on diffraction, that is, numerical wave propagation. Numerical wave propagation has been previously used in the PSDI to eliminate the effects of dust particles on phase measurements. In this application, the amplitude and phase measured at the CCD was used to back-propagate the measured wavefront to each optical surface within the PSDI to find and eliminate (in software) the effects of dust particles and defects on a measurement. These propagation codes were "first order" diffraction calculations based on Huygen's integral and implemented using the fast Fourier transform. Huygen's integral, however, makes the paraxial approximation and does not have the sub-nanometer phase accuracy required for imaging. Only recently have we

developed a way to do the scalar propagation with picometer phase accuracy that can run in a reasonable time on a desktop computer. With this new capability a lensless PSDI is possible and has been tested on one of the previously fabricated EUVL mirrors.

The unfolded layout for lensless interferometry is similar to Fig. 4 and is shown in Fig. 5. In this configuration the measurement wavefront reflected by the mirror under test propagates in free space to the CCD. There is no longer one-to-one correspondence between a point on the mirror and a pixel on the CCD, as there was with the imaging lens. The measurement wavefront interferes with the reference wavefront coming directly from the point source.

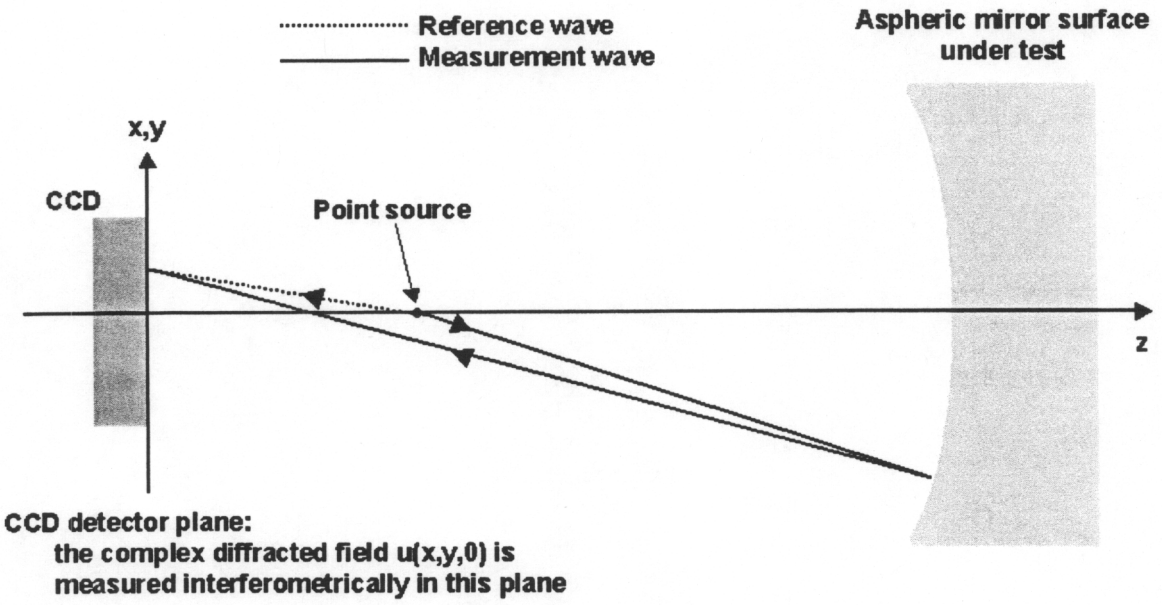

Fig. 5. Unfolded layout of a lensless PSDI.

As before, the data analysis begins with calculation of the phase and amplitude of the measurement wavefront from the recorded CCD images. This completely characterizes the complex field at the CCD. This field is now numerically propagated, in two steps, back to a fictitious spherical reference surface near the aspheric surface of the mirror under test. The first step is to add the spherical reference wave to the measured phase to get the actual phase of the measurement wave and to propagate the resultant field to the plane of the point source. The second step is the propagation of this field to the fictitious spherical reference surface located near the mirror under test. Subtracting the theoretical aspheric equation that defines the perfect mirror from the phase of this field gives the surface figure error. The two-step propagation is depicted in Fig. 6.

4. QUANTIFYING THE RESIDUAL ERROR SOURCES

To increase the accuracy of any measurement system, error sources are identified and systematically eliminated starting with the largest contributors — however, no matter how many error sources are eliminated there are always remaining ones, albeit less significant, that limit measurement accuracy. The lensless approach to phase shifting diffraction interferometry is certainly a step in the right direction with the elimination of the imaging lens and its associated errors but other errors remain. These error sources have been identified (see Fig. 7) and their magnitudes estimated by modeling and, when possible, verified experimentally. The expected accuracy of the lensless PSDI can then be estimated.

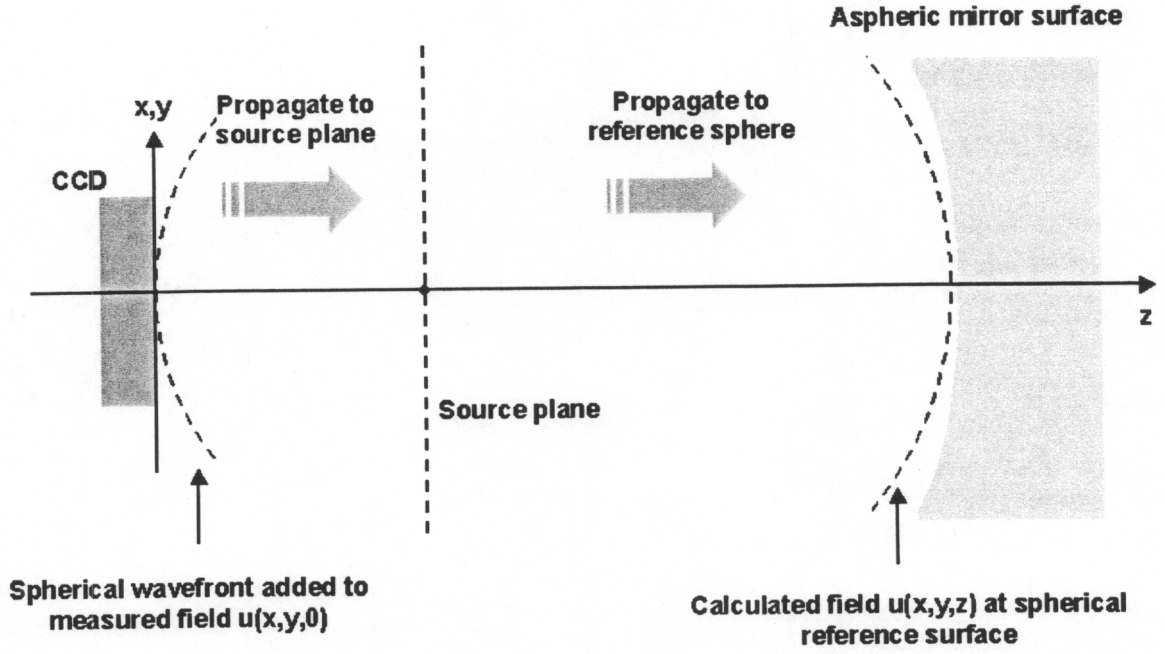

Fig. 6. Steps to numerical propagate the complex field measured at the CCD to a spherical reference near the surface of the aspheric mirror.

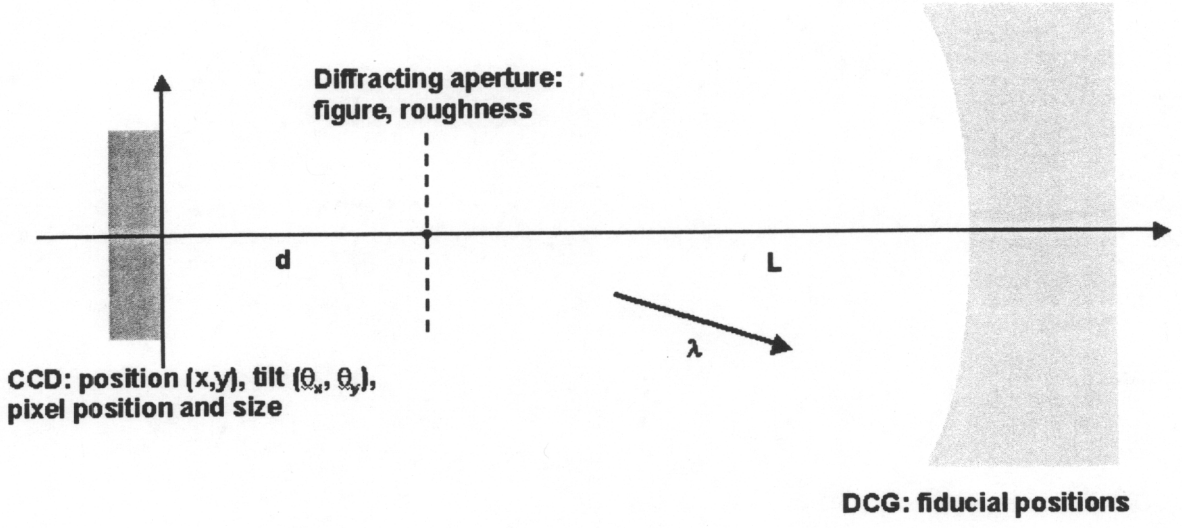

Fig. 7. Parameters of the lensless PSDI that are potential error sources.

4.1. Geometrical errors

The lensless PSDI has three components that must be aligned relative to each other. These are the mirror under test, the point source and the CCD. The geometrical relationships among these components are important to the numerical propagation calculations. Properly adding the spherical wavefront to the measured complex field at the CCD and determining the distances to propagate to the source plane and mirror under test will affect measurement accuracy. A tilt error in the CCD, for example, is equivalent to distortion when the field is propagated back to the mirror under test. Each of these errors can be simulated and/or measured in order to find the surface error contribution sensitivity as a function of each of the alignment parameters.

Before these errors can be quantified, a procedure must be defined for alignment of the lensless PSDI; this procedure includes the definition of a coordinate system. The CCD and point source uniquely define a coordinate system in the following sense: the CCD is a plane whose pixels define a two dimensional Cartesian surface **(x,y)**. The point source lies on the normal to the CCD surface at location **(0,0)**, a distance **d** from the CCD surface. The mirror under test is a distance **L** from the point source along the normal. The lensless PSDI is aligned by measuring a distortion calibration grid (DCG), which is a spherical mirror, with the same radius of curvature as the asphere to be measured, on which a set of reflective fiducials has been deposited at known coordinates. A measurement sequence consisting of a wavefront measurement and subsequent numerical back-propagation should exactly reproduce the fiducials if the coordinate origin and spacings have been chosen correctly. If not, the resultant image is out of focus and distorted. This information is used to re-align the components. After two iterations the PSDI can be aligned so there is no detectable alignment error. The DCG is then replaced with the aspheric mirror to be tested.

The mirror used for the following measurements to quantify each error source is designated M2 (S/N3) and was fabricated as a backup mirror. It has an aspheric departure of 19μm when the null fringe is positioned to minimize fringe density (not necessarily the best fit sphere). It deviates from the theoretical aspheric surface by approximately 0.5nm rms. To determine the sensitivity to misalignment, each geometrical parameter is purposely misaligned by a known amount. A measurement is taken in this state and compared to a measurement taken in the aligned state. The error sensitivity is then the surface figure difference per unit amount of misalignment. Each of the geometrical error sources is addressed below.

Induced surface figure errors due to misalignment of both **d** and **L** were measured and are shown in Fig.8.

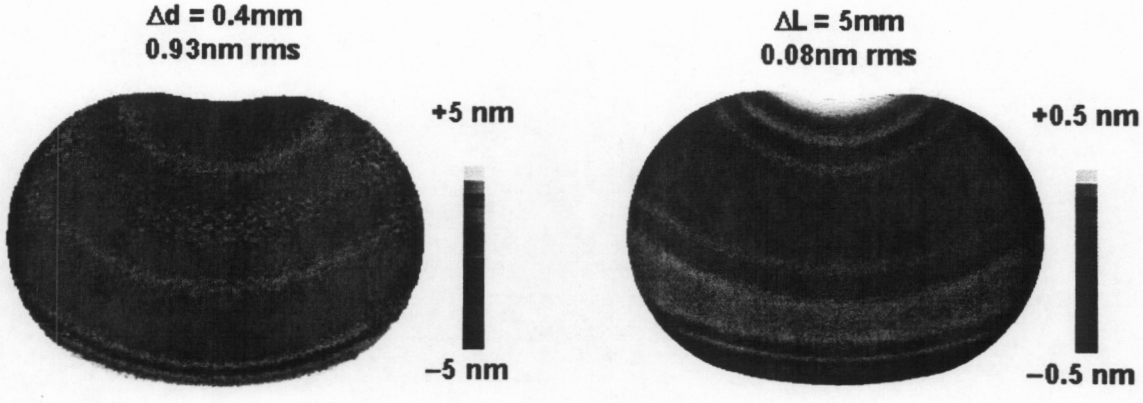

Fig. 8. Induced surface figure errors due to misalignment of the spacings between the CCD, point source and aspheric mirror.

The CCD camera can be misaligned by translation and tilt. These errors are directly related to uncertainty in the origin of the coordinate system relative to the point source and result in an error when the spherical wavefront is added to the measured complex field prior to numerical back-propagation. The induced surface figure errors are shown in Fig. 9 for each degree of freedom.

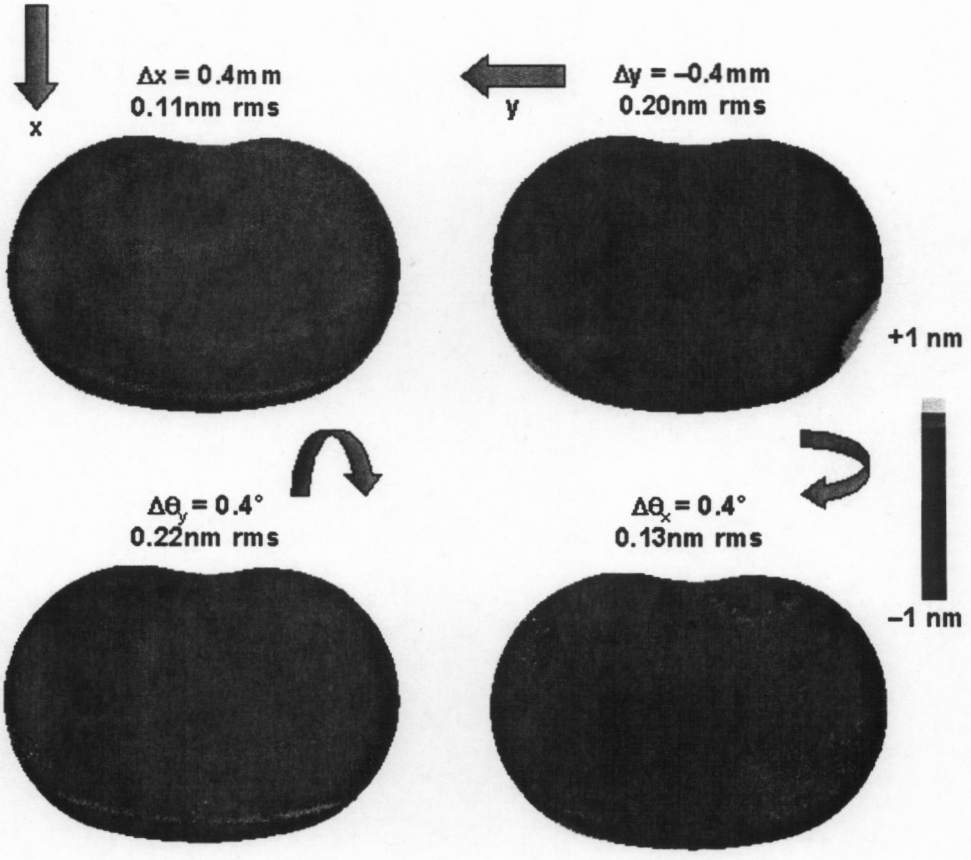

Fig. 9. Induced surface figure errors due to translation and tilt misalignments of the CCD.

4.2. CCD pixel errors

Another source of error that has not been seriously addressed in interferometry in general is the effect of a non-uniform CCD pixel grid on surface figure measurements. This grid is usually assumed to be perfect. If it is not, the coordinate system is distorted and phase measurements are assigned to incorrect coordinates. When measuring high quality spherical mirrors this error is insignificant. This is not true, however, when measuring aspheric mirrors. Fig. 10 shows the induced surface figure error when the pixel locations have a uniformly distributed error of ±0.1pixels.

Individual pixel coordinates for all 10^6 pixels on the CCD array are measured by generating a set of hyperbolic fringes from the interference of two phase-shifted spherical wavefronts. These wavefronts are produced by two optical fibers as shown in the upper half of Fig. 11. The measured phase at each pixel is compared to the theoretically computed phase. The detection centroid of each pixel is then calculated from this phase difference. The measured displacement of the pixels from a perfect square grid is shown in the lower half of Fig. 11. Once the true pixel coordinates are known for a particular CCD array, the measured phase at each pixel can be interpolated to a perfect grid before numerical back-propagation.

The actual geometric size of the CCD array is also important since absolute dimensions are necessary for characterizing aspheric optics. This size is measured with the DCG (described earlier) and its error contribution is included later in the calculation of the lensless PSDI accuracy.

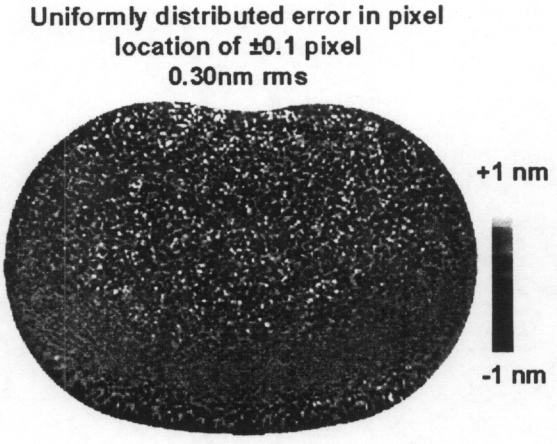

Fig. 10. Induced surface figure error due to a imperfect pixel grid.

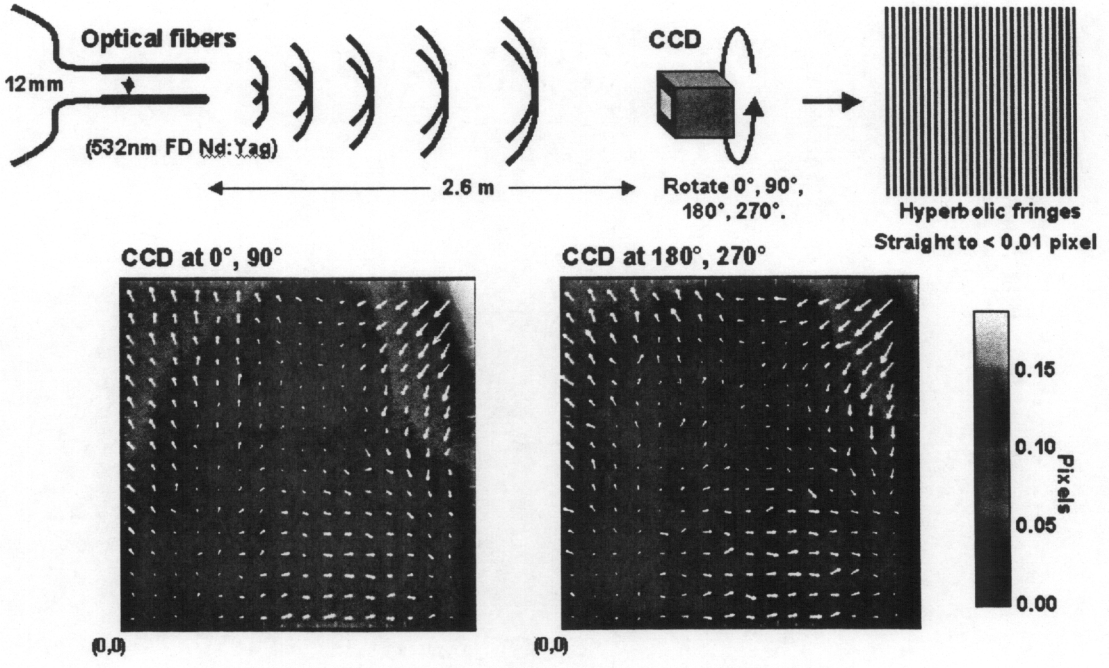

Fig. 11. Method for measuring each of the 10^6 pixel coordinates. The pixel location error for a CCD is calculated from data taken at 0° and 90°, and at 180° and 270°.

4.3. Diffraction aperture aberrations

The substrate for the diffraction aperture is a super-polished flat. The surface roughness as well as the overall flatness of the substrate can contribute an error to the surface figure measurement of an aspheric mirror. Since the wavefront reflected back to the diffracting aperture plane from the mirror only illuminates a small area in the vicinity of the diffracting aperture, low-order figure aberrations have a small effect. This is included later in the calculation of the lensless PSDI accuracy. The major effect is due to the surface roughness of the substrate. This is difficult to test experimentally because a set of diffraction apertures would have to be fabricated with different surface roughnesses. The induced PSDI measurement error can, however, be simulated. A fractal surface shown in the left half of Fig. 12, was numerically generated with a surface roughness of 0.5nm rms over the frequency range 1/mm to 1/μm. Actual data was then numerically back-propagated to the aspheric surface using both the fractal and a perfectly smooth substrate. The difference is shown in the right half of Fig. 12.

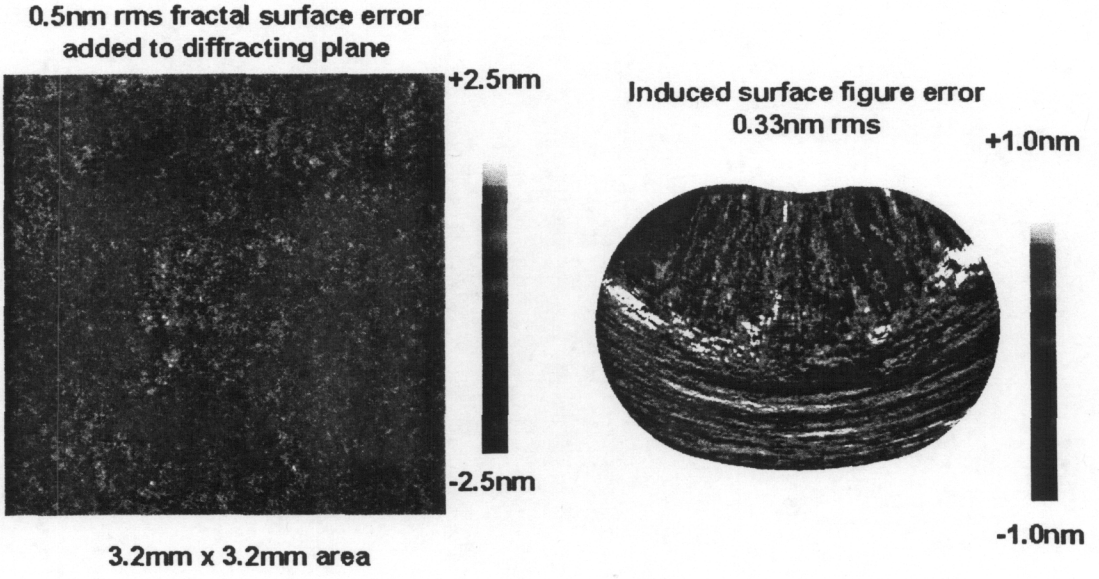

Fig. 12. A fractal surface error on the diffraction aperture indices an error in the surface figure.

4.3. Laser wavelength uncertainty

The wavelength of the laser is the basic unit of measure for most interferometry. Uncertainty in its actual value has the effect of scaling the results of a PSDI measurement as well as the numerical back-propagation since both are wavelength dependent. As mentioned earlier, the laser used in the PSDI has a sort coherence length, which implies a broad spectrum. The wavelength used in the phase calculations and numerical propagation is a weighed average of the laser spectrum. The spectrum was measured with a Jobin-Yvon spectrometer and integrated to find the centroid wavelength. A uranium discharge lamp was used as an absolute wavelength standard since it has been well characterized and has thousands of lines across the visible spectrum, several falling in the immediate vicinity of the frequency-doubled YAG laser. Fig. 13 shows the spectrum of one laser measured three times over a several hour period. The calculated centroid wavelengths are shown below the laser spectra. The calibrated uranium spectrum is superimposed on the laser spectra. All wavelengths are vacuum wavelengths.

Real data was analyzed and back-propagated using both the actual wavelength and a slightly different wavelength. The difference in the resultant surface figures, shown in Fig. 14, is the error induced by uncertainty in the wavelength.

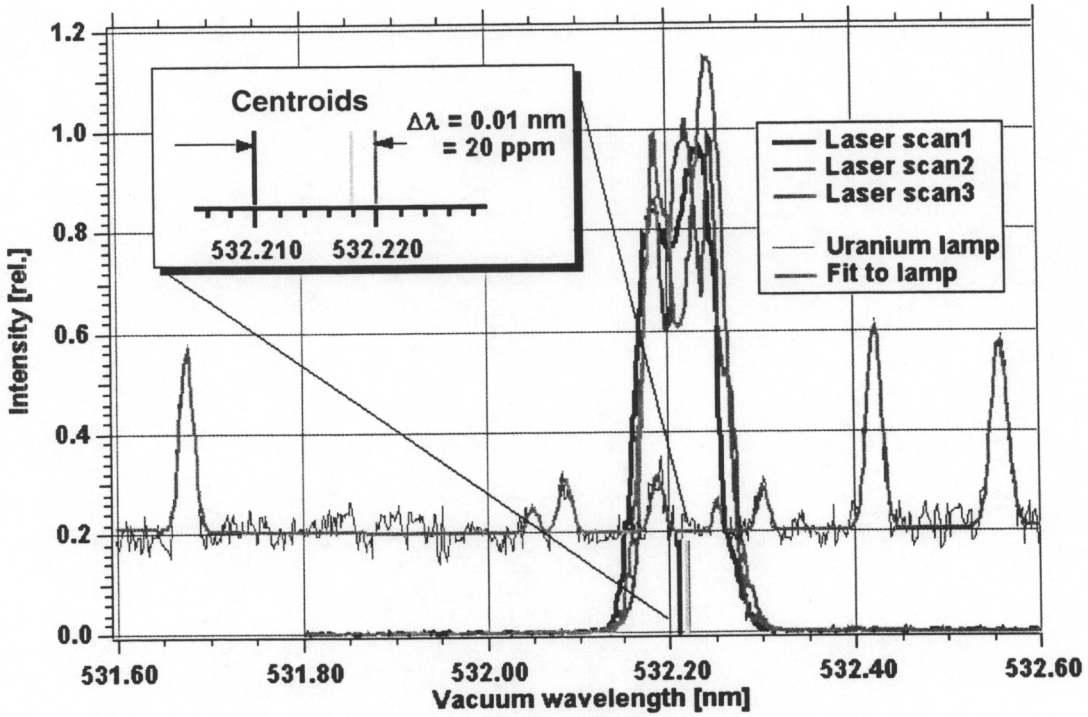

Fig. 13. A fractal surface error on the diffraction aperture indices an error in the surface figure.

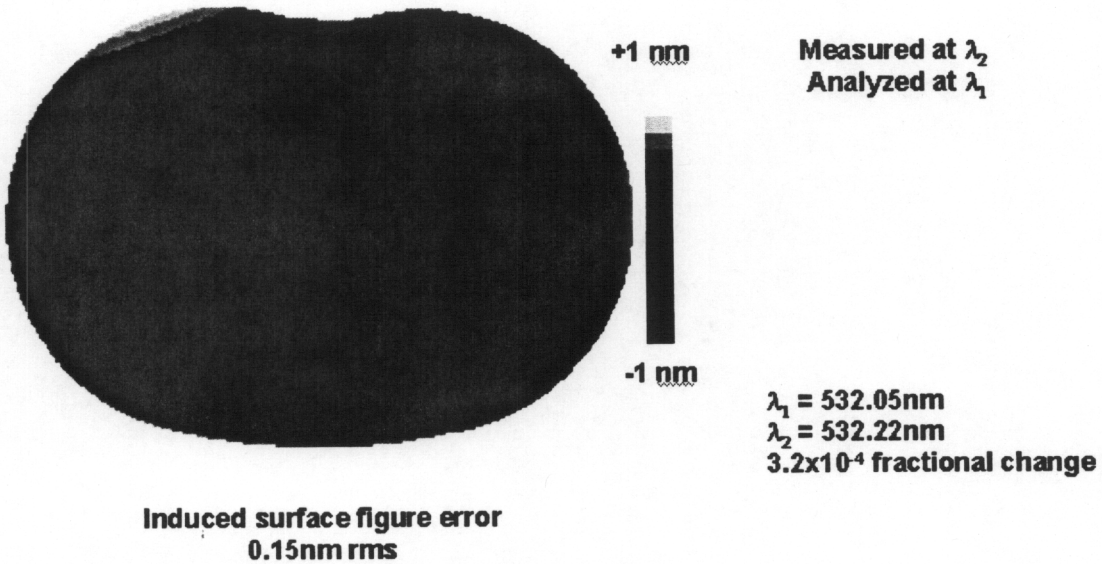

Fig. 14. A fractal surface error on the diffraction aperture indices an error in the surface figure.

5. CONCLUSIONS

The residual sources of error for the lensless PSDI have been identified and are listed in the second column of Table 1for each of the PSDI components. From modeling simulations and actual measurements, the sensitivity of the induced surface figure error has been found per unit of uncertainty for each error source. These are in the third column. Estimates of the individual errors for a well-characterized PSDI are listed in the fourth column. Finally the error contributions to the surface figure error are found by multiplying the third and fourth columns and are given in the fifth column. Assuming the errors are uncorrelated, the root-sum-squared lensless PSDI induced figure error is approximately 89pm rms.

Note that the geometrical alignment errors are the smallest contributors. The CCD pixel geometry, however, is a major source of error even after the CCD array has been carefully measured. The only other significant error is due to the diffraction aperture. Surface roughness at the 0.15nm rms (1.5Å rms) level introduces an error large enough so as to require averaging to bring it within an acceptable value.

We conclude from this work that a lensless version of the PSDI is feasible and does have the required absolute accuracy for the next generation of optics that will be needed for the six-mirror EUVL projection cameras.

Component	Source of error	Calculated figure error sensitivity	Estimated magnitude of error source	Contribution to figure error (rms)
Aspheric mirror (M2)	ΔL	16pm/mm	0.1mm	1.6pm
CCD	Δx	0.25pm/μm	2μm	0.5pm
	Δy	0.5pm/μm	2μm	1.0pm
	Δd	2.4pm/μm	2μm	4.8pm
	$\Delta\theta x$	220pm/°	0.01°	2.2pm
	$\Delta\theta y$	130pm/°	0.01°	1.3pm
	Pixel position	3000pm/pixel	0.01pixel	30pm
	Pixel size	0.6pm/ppm	100ppm	60pm
Diffracting aperture	roughness	660pm/nm	0.15nm	50pm*
	curvature	298pm/λ	λ/20	14.9pm
Laser	$\Delta\lambda$	882pm/nm	0.01nm	8.8pm
DCG	Fiducial positions	12.5pm/μm	2.0μm	25pm

* assumes four rotational averages

Total lensless PSDI error (RSS) = 89pm rms

Table 1. Summary of all error contributions and the root-sum-squared (RSS) assuming the errors are uncorrelated.

REFERENCES AND NOTES

1. G.E. Sommargren, "Phase shifting diffraction interferometry for measuring extreme ultraviolet optics," OSA Trends in Optics and Photonics Vol. **4**, Extreme Ultraviolet Lithography, Glenn D. Kubiak and Don R. Kania, eds. (Optical Society of America, Washington, DC 1996), pp. 108-112.
2. Phase shifting can also be accomplishment by axially translating the fiber or aspheric mirror, but the phase shift is non-uniform across the spherical wavefronts.
3. D.W. Phillion, "General methods for generating phase-shifting interferometry algorithms," Appl. Opt. **36**, 8098-8115 (1997).
4. Sommargren, G.E., Phillion, D.W., Campbell, E.W., "Sub-nanometer interferometry for aspheric mirror fabrication," *Precision Science and Technology for Perfect Surfaces*, Y. Furukawa, Y. Mori and T. Kataoka, Editors, (Japan Society for Precision Engineering, Tokyo, 1999) pp. 329-335.

ACKNOWLEDGMENTS

This work was performed by the University of California Lawrence Livermore National Laboratory under the auspices of the U.S. Department of Energy, Contract W-7405-Eng-48. Funding was provided by the EUV LLC under a Cooperative Research and Development Agreement.